

# Design of Optimal Wing–Body Configuration to Delay Onset of Vortex Asymmetry

Jinsheng Cai\*

*Northwestern Polytechnical University, 710072 Xi'an, People's Republic of China*

Her-Mann Tsai†

*Science Centre Singapore, Singapore 609081, Republic of Singapore*

and

Shijun Luo‡ and Feng Liu§

*University of California, Irvine, Irvine, California 92697-3975*

DOI: 10.2514/1.J050595

**The stability analysis previously developed by the authors is augmented by a numerical conformal mapping technique in order to extend its applicability to problems with complex geometry. The extended method is applied to investigate the stability of symmetric vortices over wing–body combinations with various designs of the cross-sectional geometry through morphing of a basic profile formed by a flat-plate delta wing and a circular-cone centerbody. The effect of the thickness of the wing and the body, the bending of the wingtips, and the contouring of the cross-sectional profiles of the wing and the body are summarized. It is discovered that a cross-sectional profile resembling that of a disturbed cobra has the largest stability range, up to very high angles of attack, for the symmetric vortices over a slender conical forebody.**

## I. Introduction

ONE important phenomenon associated with high-angle-of-attack aerodynamics is the sudden onset of vortex asymmetry on the forebody of an air vehicle in symmetric flight. One of the first observations of the onset of vortex asymmetry was reported in 1951 by Allen and Perkins [1]. Interest in the phenomenon has been intensified since the late 1970s as concepts for highly maneuverable aircraft have been developed. These high-performance aircraft are expected to operate routinely at angles of attack at which vortex asymmetry is likely to occur. When vortex asymmetry occurs, the aerodynamic, stability, and control characteristics of the vehicle change dramatically. In the meantime, the conventional aerodynamic controls become ineffective due to the vortex wakes generated by the forebody. The subject was reviewed by Hunt [2], Ericsson and Reding [3], and Champigny [4].

High-angle-of-attack flow control is most effective when applied in the region close to the tip of the forebody. The presence of two closely spaced vortices around the pointed forebody at high angles of attack enhances the effectiveness. Compared with that on wings, control on the forebody is required over a much smaller area; thus, physical requirements such as size and weight should be much smaller. The lengthy forebody of a modern fighter further enhances the control effectiveness by providing a long moment arm. Excellent reviews of this activity can be found in papers by Malcolm [5,6] and Williams [7]. Recently, Liu et al. [8] successfully demonstrated linear proportional control of the side forces over a slender circular cone using duty-cycled single-dielectric-barrier-discharge plasma actuators.

One of the devices to suppress the flow asymmetry are the horizontal nose strakes. Coe et al. [9] showed, by wind-tunnel tests,

the alleviating effects of horizontal and symmetrical strakes placed close to the apex of a slender ogive forebody and a slender circular cone. It is observed that the effect of the strakes is to produce a well-defined point of separation at the leading edges of the strakes, which results in a symmetrical flowfield over a wide range of high angles of attack. Two sharp side edges on an otherwise smooth body can also serve to define the point of separation. Siclari [10] used a Navier–Stokes solver to study the natural occurrence of separated flows over biparabolic and biwedge cones at a freestream Mach number of 1.8 and an angle of attack of  $20^\circ$ . As the thickness ratio was increased, the originally symmetric vortex pair separated from the sharp side edges, becoming asymmetric at thickness ratios of 0.5 and 0.6 for the biparabolic and biwedge cones, respectively.

Cai et al. developed a stability analysis method [11] and used it to study high angle-of-attack flow about slender conical wing and wing–body combinations [12,13]. The analytic method is based on an eigenvalue analysis on the motion of the vortices under small temporal perturbations. The theoretical results agree well with available experimental observations and are corroborated by numerical computations [14].

The aim of the present paper is to manipulate the aerodynamic configuration for the purpose of keeping the stationary symmetric vortex pair stable at high angles of attack. In the following sections, the analytic method in [11] is summarized and a numerical conformal mapping technique is described. A series of configurations are analyzed for the stability of the symmetric vortex pair. A most effective configuration of the wing–body combination is obtained by the analytic method and validated by an Euler solver. In the last section, conclusions are drawn.

## II. Theoretical Method

In this section, the vortex-flow model and the stability analysis developed in [11] are summarized. Semiempirical modifications to the model are made to account for the effects of the vortex core [15]. A numerical conformal mapping technique is used to obtain solutions for almost arbitrary wing–body combination cross sections.

### A. Vortex Velocity Expression

Consider the flow past a slender conical wing–body combination at an angle of attack  $\alpha$  and sideslip angle  $\beta$ , as shown in Fig. 1. The sideslip angle  $\beta$  is taken to be zero for the present study. The velocity

Received 6 April 2010; revision received 3 September 2010; accepted for publication 23 September 2010. Copyright © 2010 by the authors. Published by the American Institute of Aeronautics and Astronautics, Inc., with permission. Copies of this paper may be made for personal or internal use, on condition that the copier pay the \$10.00 per-copy fee to the Copyright Clearance Center, Inc., 222 Rosewood Drive, Danvers, MA 01923; include the code 0001-1452/11 and \$10.00 in correspondence with the CCC.

\*Professor, National Key Laboratory of Aerodynamic Design and Research.

†Scientist, 15 Science Park Road. Senior Member AIAA.

‡Researcher, Department of Mechanical and Aerospace Engineering.

§Professor, Department of Mechanical and Aerospace Engineering. Associate Fellow AIAA.

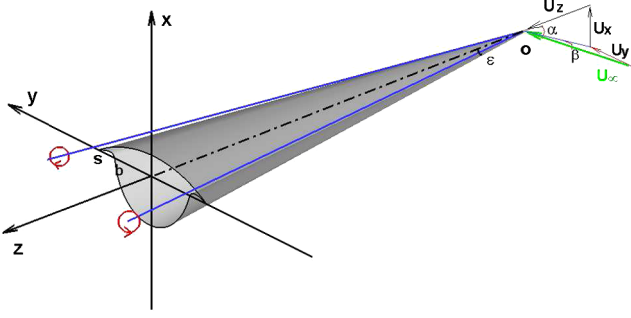


**Fig. 1 Slender conical wing-body combination and separation vortices.**

of the freestream flow is  $U_\infty$ . The planform of the wing has a half-vertex angle of  $\epsilon$ . In a cross-sectional plane at  $z$ , the wing has a half span  $s$ , and the centerbody has a half span  $b$ . The wing-body combination is assumed to be conical and of infinite length. No effects of trailing edge or body base are considered.

At high angles of attack, separation vortices from the leading edges of the wing form two vortex sheets, which roll up into two separate concentrated vortex cores, shown in Fig. 1 (vortex sheets not shown). The strengths of the vortex cores grow linearly with downstream distance, because the leading-edge vortex sheets feed into the vortex cores. The flow is irrotational except within the vortex sheets and the concentrated vortex cores. The problem can be solved by solving the three-dimensional Laplace equation with the distribution of discrete vortices subject to the boundary condition of zero normal flow velocity on smooth body surfaces and the Kutta condition at sharp edges. By the principle of superposition, the flow around a slender body can be obtained by solving the following two flow problems: 1) the flow due to the normal components of the freestream velocity,  $U_x = U_n = U_\infty \sin \alpha$  and  $U_y = 0$ ; and 2) the flow due to the axial component of the freestream velocity,  $U_z = U_\infty \cos \alpha$ .

To study the stability of the vortex flow, a simplified vortex model due to Legendre [16] is adopted here. The Legendre model consists of one pair of concentrated vortices emanating from the apex of the body, as shown in Fig. 1. The distributed vortex sheets that connect the leading edges and the two concentrated vortices are neglected in this model. More accurate models employing the use of discrete vortex sheets and the general discrete vortex method may be used and necessary for accurate prediction of aerodynamic performance characteristics, but the simplicity and the analytical nature of the resulting solution method of the Legendre model outbalance the benefit of a more complex method in the present study. In this simplified model, the two concentrated vortices are assumed to be conical rays from the body apex  $O$ . Secondary separation vortices, if any, are weak and thus also neglected. Vortex breakdown is not considered. The flow is then assumed to be steady, inviscid, incompressible, conical, and slender.

With the previous simplifications, the first flow problem in the decomposition of the original three-dimensional problem reduces to a two-dimensional problem, which can be solved by using a conformal mapping  $\zeta = \zeta(Z)$  that maps the body contour in the plane  $Z = x + iy$  to a circle of unit radius in a uniform flow of velocity  $(U_x, U_y)$  in the plane  $\zeta = \xi + i\eta$ . The two concentrated vortex cores are represented by two point vortices in the crossflow plane  $(x, y)$ , for which the strength (circulation around the point vortex) is denoted by  $\Gamma$ , which varies linearly with axial distance from the body apex. The second problem is solved by the condition of conical flow, in which the flow is invariant along rays emanating from the apex. Details of the mathematics are given in [11].

Experimental measurements and computational data both show significantly increased axial flow velocity along the vortex cores, which results in a suction effect of the flow toward the vortex core. To account for this effect, a sink of strength  $Q_c$  is added to each vortex  $\Gamma$ , and the freestream velocity component along the body axis  $U_z$  used in the second flow problem is augmented by a factor  $(1 + K_c)$ , where

$K_c > 0$ .  $Q_c$  and  $K_c$  are related to the strength of the vortex considered  $\Gamma$  by a semiempirical method.  $Q_c = -q_c \Gamma$  and  $K_c = \kappa[\Gamma/(2\pi s U_x)]^2$ , where  $q_c = 0.02$  and  $\kappa = 0.3$ . The development of this model and the selection of the values of  $q_c$  and  $\kappa$  are based on comparisons with available experimental measurements and full Euler computations of representative configurations. Reference [15] gives the details of the derivations and verifications.

Let  $Z_1$  (or  $\zeta_1$  on the transformed plane) be the location of the first vortex. Following [12,15], the complex velocity at  $Z_1$  is as follows:

$$\begin{aligned} u_1 - iv_1 = & \left[ \left( \bar{U}_n - \frac{U_n}{\zeta_1^2} \right) + \frac{i\Gamma_1}{2\pi} \left( -\frac{1}{\zeta_1 - 1/\bar{\zeta}_1} \right) \right. \\ & - \frac{i\Gamma_2}{2\pi} \left( \frac{1}{\zeta_1 - \zeta_2} - \frac{1}{\zeta_1 - 1/\bar{\zeta}_2} \right) - \frac{q_c \Gamma_2}{2\pi} \left( \frac{1}{\zeta_1 - \zeta_2} \right. \\ & \left. \left. + \frac{1}{\zeta_1 - 1/\bar{\zeta}_2} - \frac{1}{\zeta_1} \right) - \frac{q_c \Gamma_1}{2\pi} \left( \frac{1}{\zeta_1 - 1/\bar{\zeta}_1} - \frac{1}{\zeta_1} \right) \right] \left( \frac{d\zeta}{dZ} \right)_1 \\ & - \frac{(i - q_c)\Gamma_1}{4\pi} \left( \frac{d^2 Z}{d\zeta^2} \right)_1 \left( \frac{d\zeta}{dZ} \right)_1^2 - \frac{(1 + K_{c1})U_x \bar{Z}_1}{sK} \\ & + \frac{1}{2\pi} \sum_{j=1}^N \frac{Q_j}{Z_1 - Z_{Qj}} \end{aligned} \quad (1)$$

where the overbar denotes complex conjugate;  $K = \tan \alpha / \tan \epsilon$  is the Sychev [17] similarity parameter, originally identified as a similarity parameter for hypersonic flows. Hemsch [18,19] and Barnwell [20] showed later that Sychev's similarity [17] could also be extended to low supersonic, transonic, and subsonic slender-body flows. Hemsch and Luckring [21] also showed the connection between the strength of the vortex  $\Gamma$ ,  $\epsilon$ , and  $K$ . It must be pointed out that at sufficiently large angle of attack, the flow will cease to be conical. The vortices may become spiral before vortex breakdown occurs. Traub [22] developed a method to predict the onset of vortex breakdown, as related to  $K$  and  $\epsilon$ , on delta wings using the correlation by Hemsch and Luckring [21].

The last two terms on the right-hand side of Eq. (1) are the solution to the flow problem 2, and the other terms are the solution to the first flow problem.  $Q_j$  ( $j = 1, 2, \dots, N$ ) are the strengths of the point sources at the points  $Z_{Qj}$  to be determined by  $N$  simultaneous equations of the boundary conditions at  $N$  points on the body contour in the augmented axial flow. The subscript 1 denotes the values at vortex point  $Z_1$  (or  $\zeta = \zeta_1$ ). A similar expression is obtained for the complex velocity at the center of the other vortex denoted by  $Z_2$  (or  $\zeta_2$ ).

Only vortex configurations (locations and strengths of the vortices) that result in zero flow velocities at the two vortex centers can exist in a steady flow. These locations of the vortices are called the stationary positions. The stationary positions  $Z_1$  and  $Z_2$  and the strengths  $\Gamma_1$  and  $\Gamma_2$  of the two vortices in the previous model are determined by solving a set of four algebraic equations by a Newton iteration method [13]. Only symmetric stationary vortex positions are considered in this paper.

## B. Numerical Conformal Mapping

The method of numerical conformal mapping by James [23] and Halsey [24] is used here. The cross sections considered have two sharp edges at points  $Z_A$  and  $Z_B$  with the same included angle  $\nu$  and are smooth elsewhere. Two steps are adopted to map the body contour in the plane  $Z = x + iy$  to a circle of unit radius in uniform flow of velocity  $(U_x, U_y)$  in the plane  $\zeta = \xi + i\eta$ .

Step 1 is a corner-removing mapping. The Karman-Trefftz transformation is used to map the body contour with corners in the plane  $Z$  to a smooth contour in the plane  $\chi$ :

$$\frac{Z - Z_A}{Z - Z_B} = \left( \frac{\chi - \mu Z_A}{\chi - \mu Z_B} \right)^{1/\mu} \quad (2)$$

where  $\mu = 1/(2 - \nu/\pi)$ .

Step 2 is a smooth-contour-to-unit-circle mapping. The function to map the smooth contour in the plane  $\chi$  to the unit circle in the plane  $\zeta$  is expressed in an infinite series form:

$$\chi = \zeta + c_0 + \frac{c_1}{\zeta} + \frac{c_2}{\zeta^2} + \dots \quad (3)$$

where  $c_0, c_1, c_2, \dots$  are constant complex numbers to be calculated numerically.

### C. Stability Under Small Perturbations

When a vortex pair is slightly perturbed from their stationary positions and then released, motion of each vortex follows the vortex velocity, as given by Eq. (1). Its coordinates as functions of time are governed by a system of two first-order ordinary differential equations. Once the vortex velocity given by Eq. (1) is found, the two eigenvalues  $\lambda_1$  and  $\lambda_2$  of the ordinary differential equations can then be easily computed to determine the stability of the vortex. Details of theory and computational methods are given in [11]. The method has been validated against a number of wing, body, and wing-body combination cases through comparisons with experiments and computations in [11–13].

The eigenvalues  $\lambda_1$  and  $\lambda_2$  depend on the Sychev similarity parameter  $K$ , which is essentially the ratio of the angle of attack to the body apex angle, and other geometric parameters; e.g., the wing-body span ratio  $\gamma = b/s$ . Any perturbation of the stationary positions of the vortex pair can be decomposed into a symmetric perturbation and an antisymmetric perturbation. The maximum real part of the two eigenvalues  $\lambda_1$  and  $\lambda_2$  for each vortex of the stationary vortex pair under small symmetric or antisymmetric perturbations is used to determine stability in this analysis. A positive value of this variable means growth of the perturbation (unstable), a negative value means decay of the perturbation (stable), and a zero value means that the perturbation remains unchanged (neutrally stable). A vortex pair is stable if, and only if, both vortices are stable under both symmetric and antisymmetric perturbations.

## III. Vortex Control by Morphing the Wing-Body Cross Section

The symmetric vortex pair over a series of representative wing, body, and wing-body combination topologies at high angles of attack is studied. The stationary symmetric vortex positions are solved, and then their stability under small symmetric and antisymmetric perturbations is investigated by the previously mentioned analytic method. These investigations guide us to a design of a wing-body configuration that is most effective for suppressing flow asymmetry up to a very high angle of attack.

### A. Bending the Wingtips Upward or Downward

It has been shown that the symmetric vortex pair over a slender flat-plate delta wing is stable at any angle of attack before vortex breakdown by experiments [25] and analyses [11,26]. An actual wing must have a finite thickness. Increased thickness is found to reduce the critical angle of attack for vortex asymmetry. The effect of bending the tips of a wing upward or downward with finite thickness is investigated in this subsection.

#### 1. Bending the Wingtips Upward

Figure 2a plots the cross section of a conical wing of finite thickness with the tips bent upward. The upper and lower cross sections are defined by two circular arcs,  $x = x_c - (r_c^2 - y^2)^{1/2}$ . For the upper surface, the center of the circular arc is located at  $x_c/s = 1.9633$ , and the radius  $r_c/s = 2.2033$ . For the lower surface,  $x_c/s = 1.5166$ , and  $r_c/s = 1.8166$ . The maximum thickness is  $0.060s$ . The stationary locations of the symmetric vortices over this wing are computed and shown as the circle symbols in Fig. 2a for a number of angle of attacks represented by the Sychev parameter ranging from 1.0 to 8.0 at an interval of 0.5. The stationary symmetric vortices are located well inboard the wing and move upward and a little further inboard as the angle of attack is increased.

The maximum real part of the eigenvalues of the symmetric vortex pair under small symmetric and antisymmetric perturbations are computed and plotted in Fig. 2b for the same  $K$  values. The symmetric vortex pair is stable when  $K < 2.755$  and unstable otherwise. The same analysis is performed for a wing without bending but with the same thickness (bicircular cross section). It yields that the stable-to-unstable transition  $K$  is beyond  $K = 8.0$ . In comparison with a flat-plate delta wing, for which the critical  $K$  is infinity, nonzero thickness destabilizes the symmetric vortex pair over a slender conical wing, and upward bending further destabilizes the vortices.

#### 2. Bending the Wingtips Downward

If we flip the previous wing upside down, we achieve a conical wing of the same thickness with the sharp leading edges bent downward. The cross-sectional shape, the location of the vortices, and their stability analysis results are shown in Fig. 3, in the same format as before. Compared with the upward-bending case, the vortices are now located further outboard, nearly along the vertical lines passing through the wingtips. When  $K$  is near 1.0, the vortex lies very close to the upper curved surface of the wing and near the leading edge from where it is separated.

In contradiction with the upward-bending case, bending down the wingtips has increased the stable-to-unstable transition critical  $K$  to beyond the computed  $K = 8.0$  range. However, the vortices become unstable for  $K < 3.188$ . The extended stability range for large  $K$  compared with the upward-bending case is related to the increased distance and thus reduced interaction between the vortex pair when

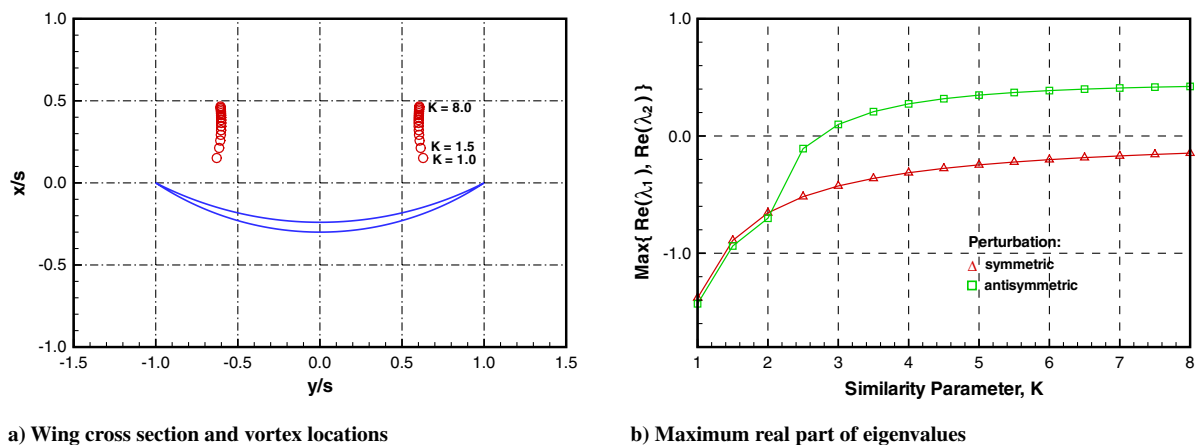
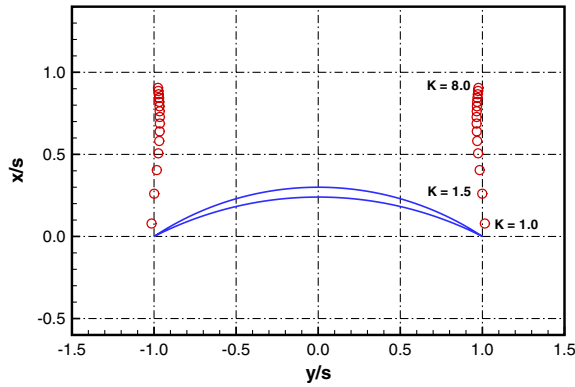
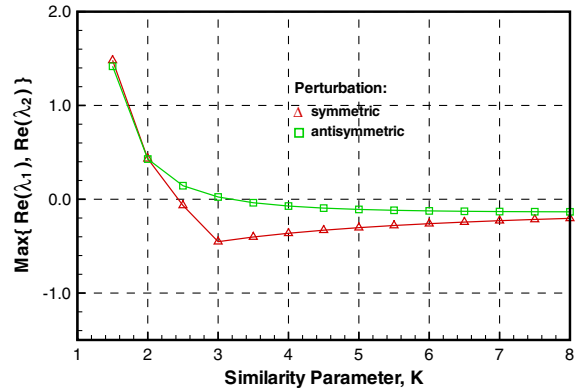


Fig. 2 Wing with the tips bent upward.



a) Wing cross section and vortex locations



b) Maximum real part of eigenvalues

Fig. 3 Wing with the tips bent downward.

the tips are bent downward. The unstable behavior when  $K$  is small appears to be related to the extraordinarily close proximity and thus strong interaction between the vortices and the wing surface, as shown in Fig. 3a.

We thus conclude that bending the wingtips downward has a favorable effect on keeping the flow symmetry for large  $K$ , but the effect is unfavorable when  $K$  is small. To make use of the favorable effect, the destabilizing effect at low values of  $K$  needs to be eliminated. This can be done by a local configuration modification, to be shown in Sec. III.C.

### B. Volume Distribution of a Body with Sharp Side Edges

The body is always required to have a specified volume. The configuration considered in this subsection has two symmetric sharp side edges, and the horizontal plane passing through the two edges divides the body volume into the upper and lower parts. The sharp edges on the body surface determine the separation locations of the vortices.

#### 1. Larger Upper Volume

The contour of the body is specified by two scaled circular arcs defined by  $x = \sigma[x_c - (r_c^2 - y^2)^{1/2}]$ , where  $\sigma$  is a scale parameter. For the lower surface,  $\sigma = 1.0$ ,  $x_c/s = 1.5166$ , and  $r_c/s = 1.8166$ . For the upper surface,  $\sigma = 2.3332$ ,  $x_c/s = -1.5166$ , and  $r_c/s = 1.8166$ . This gives a thick top surface ( $x/s = 0.70$ ) and a thin lower surface ( $x/s = -0.30$ ). Figure 4a shows the body cross-sectional shape and the computed locations of the stationary symmetric vortex pair over the body again for the Sychev parameter  $K$  range from 1.0 to 8.0 at an interval of 0.5. The corresponding eigenvalues for the perturbations of the vortex system are plotted in Fig. 4b.

The vortex pair is located slightly outboard of the body and moves upward away from the sharp edges as  $K$  increases. These vortices are

unstable for all values of  $K$ . The larger upper volume destabilizes the symmetric vortex pair. The destabilization may be related to the increased interaction between the vortices and the protruding upper body.

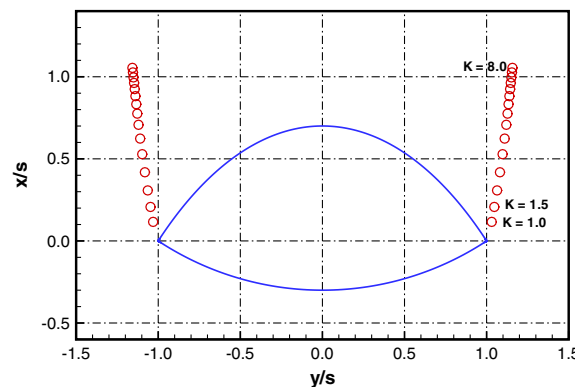
#### 2. Larger Lower Volume

If the body of the previous discussion (Fig. 4) is turned upside down, the lower volume becomes larger than the upper volume, as shown in Fig. 5. The vortices are now located slightly inboard. They move upward as  $K$  increases. Figure 5b shows that the stationary symmetric vortex pair is stable when  $K < 3.742$ , and unstable otherwise in this case.

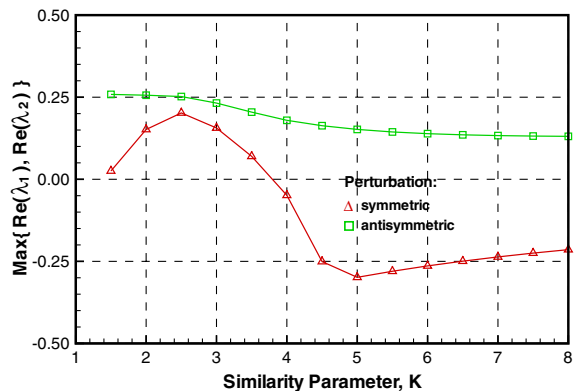
We therefore conclude that, for the same total volume, a body with a larger lower volume is favored over a body with a larger upper volume for vortex stability. The forebody of the high-performance fighter F-22 has a shape similar to Fig. 5a rather than that of Fig. 4a. According to the present analysis, this configuration exhibits stable stationary symmetric vortex behavior until a rather high angle of attack.

### C. Moving the Wingtips Upward or Downward in a Wing-Body Combination

We now evaluate wing-body combinations. We attach a conical wing, discussed in Sec. III.A, to a circular cone at the midposition, as shown in Figs. 6a or 7a. The cone-width-to-wingspan ratio is  $\gamma = 0.7$ . The cross section of the wing has a maximum thickness  $0.04s$  at the wing root. The small wing may be viewed as strakes to help stabilize the vortices over the body. The sharp leading edges of the wing are bent  $h$  distance away from the horizontal plane (positive when upward). To facilitate the numerical conformal mapping of the cross section of the wing-body combination, the sharp corners formed at the conjunctions of the wing and body are rounded by a

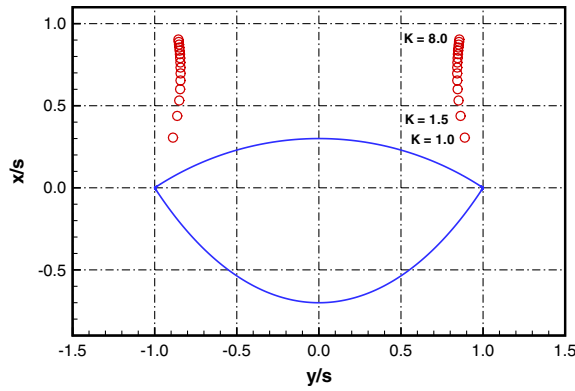


a) Body cross section and vortex locations

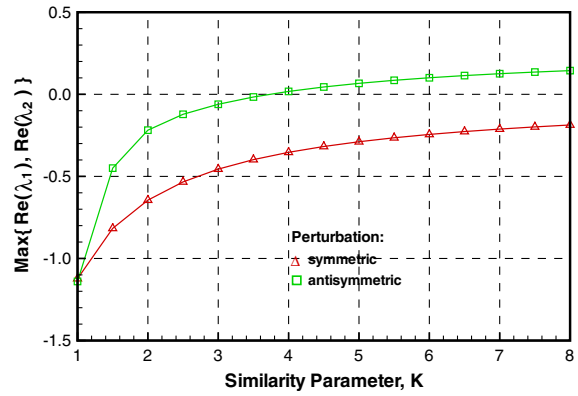


b) Maximum real part of eigenvalues

Fig. 4 Body with large upper volume and sharp side edges.



a) Body cross section and vortex locations



b) Maximum real part of eigenvalues

Fig. 5 Body with large lower volume and sharp side edges.

second-order smoothing technique so that only the two leading edges remain sharp in the entire contour of the wing-body cross section. This remark holds true for all wing-body combinations considered in this paper.

1. Curved Wing with Upward Tips

Figure 6a depicts the contour of the wing-body combination with the wingtips moved upward at  $h/s = 0.2$  and the computed locations of the stationary symmetric vortex pair. Similar to the wing-alone case, the vortex pair lies well inboard of the wingtips. It moves upward along nearly vertical lines with increasing  $K$ . The upward movement is not uniform with respect to the increase of  $K$ . When  $K$  increases from 2.0 to 2.5, the upward movement is rather abrupt. This is caused by the corner formed by the wingtip and the cone. Once  $K$  is sufficiently large, the vortex pair moves out from the corner area. When  $K$  lies in the intervals (1.0, 2.0) and (6.0, 8.0), the vortex upward movement is hardly seen.

Figure 6b shows the maximum real part of the eigenvalues for this configuration. The symmetric vortex pair is stable for all  $K < 2.1$  and unstable otherwise. The stable-to-unstable transition appears to coincide with the abrupt upward movement of the vortex pair. Additional analyses show that the critical  $K$  value decreases when  $h/s$  increases. Therefore, the upward movement of the wingtips destabilizes the symmetric vortex pair over the this wing-body combination, as is the case for the wing-alone configuration.

2. Curved Wing with Downward Tips

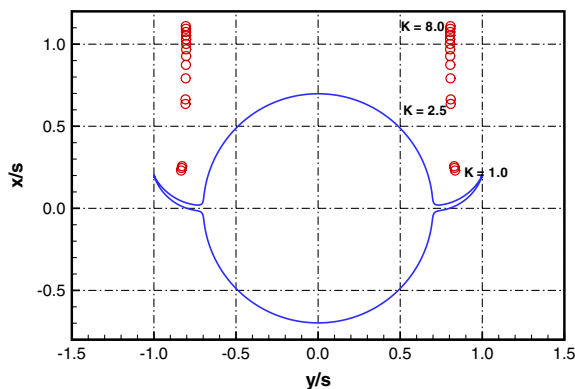
Consider the same wing-body combination of Fig. 6 but with the wingtips moved downward at  $h/s = -0.2$ , as shown in Fig. 7a. The vortices lie outboard of the wing and move upward and further outboard with increasing  $K$ . This helps to stabilize the vortices for large  $K$ . The vortex movement with  $K$  is smooth, except when  $K$

increases from 1.0 to 1.5. When  $K = 1.0$ , the vortices lie very close to the curved upper surface and near the leading edges. As discussed in Sec. III.A, a destabilizing effect near  $K = 1.0$  is expected because of the close proximity of the vortices to the wingtips. Figure 7b shows the eigenvalues for this configuration. The symmetric vortex pair is found to be stable for  $1.968 < K < 5.025$  and unstable otherwise. Similar to the wing-alone case with a downward-bent tip, the symmetric vortex pair for the wing-body combination is unstable when  $K$  is low. But contrary to the wing-alone case, the stable symmetric vortex pair becomes unstable when  $K$  is large because of the destabilizing effect of the large volume of the centerbody [11].

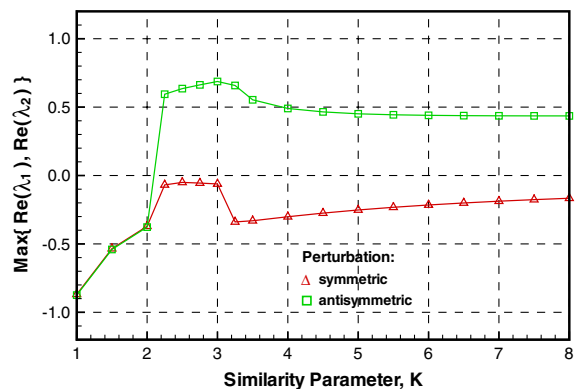
3. Straight Wing with Downward Tips

The curved wing with tips moved downward has an effect of destabilizing the symmetric vortex pair for small values of  $K$  in either the wing-alone case or when combined with a centerbody. When  $K \approx 1.0$ , the stationary symmetric vortices lie very close to the convex upper surface of the wing and near the leading edges. The instability of the symmetric vortices appears to be caused by the strong interaction between the vortices and the convex surface of the wing. From experience, this instability situation at low  $K$  can be altered by a local geometry modification of the wing. To realize this, the curved wing with a convex upper surface in the previously mentioned wing-body combination study is replaced by a wing with planar upper and lower surfaces with the same root thickness and tip downward displacement. The resulting cross-sectional profile, the computed stationary vortex pair locations, and the corresponding eigenvalues are shown in Fig. 8.

Employment of the planar wing surfaces significantly raises the location of the stationary symmetric vortices at  $K = 1.0$  in comparison with the previously mentioned convex wing surface case. The positions for other values of  $K$  remain nearly unchanged.

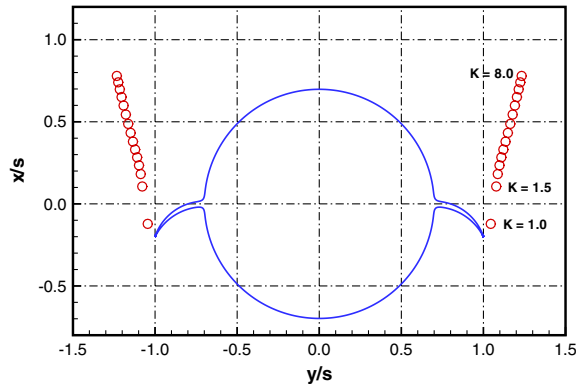


a) Wing-Body cross section and vortex locations

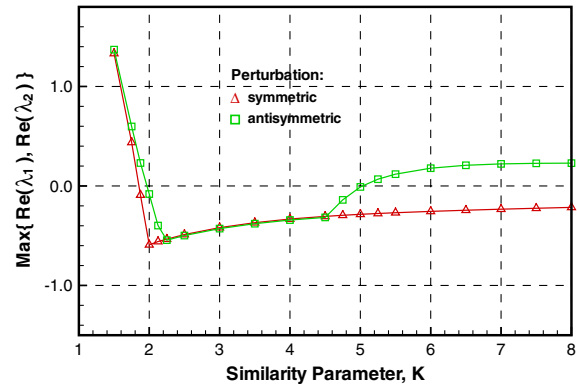


b) Maximum real part of eigenvalues

Fig. 6 Wing-body combination with the wingtips moved upward.



a) Wing-Body cross section and vortex locations



b) Maximum real part of eigenvalues

Fig. 7 Wing-body combination with the wingtips moved downward.

Figure 8b indicates that the instability of the vortices at the low  $K$  values are now completely eliminated. The critical value of  $K$  above which the vortices become unstable is now  $K = 4.762$ , only slightly smaller than the case with convex wing surfaces. More detailed comparisons for different  $h/s$  values of the convex and planar wing cases are presented in [27].

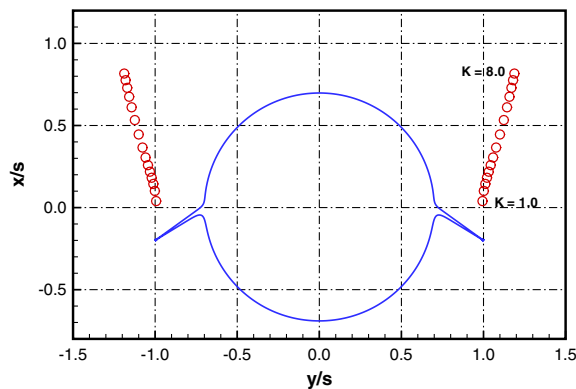
We thus see that downward movement of the wingtips of a curved wing is favorable at high angles of attack against upward movement but unfavorable at low angles of attack. This destabilizing effect can be eliminated while keeping the favorable stability behavior at high  $K$  values by straightening the curved surface of the wing.

**D. Disturbed-Cobra Forebody**

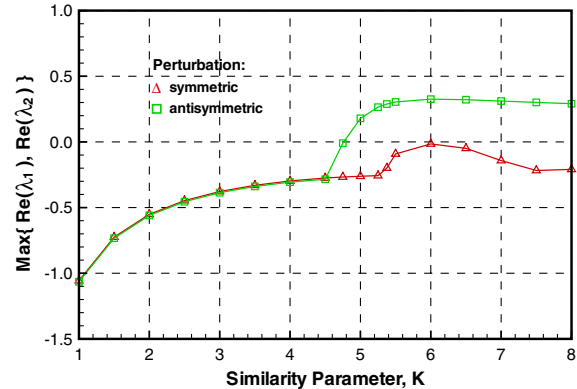
The previous investigations, along with experience gained by the authors in studying various other profiles, lead us to design a wing-body combination shape that consists of a centerbody with a flat top and downward-pointing straight strakes (wing). Both the reduced upper volume of the body and the downward-pointing strakes help stabilize the vortices at high angles of attack (high  $K$  value). The use of planar top and lower surfaces of the strakes removes the instability at the very low angles of attack ( $K$  close to 1.0).

We thus conceive a wing-body combination, as shown in Fig. 9a, which resembles the shape of the head of a disturbed cobra. The upper contour of the wing is formed with an elliptic arc smoothly connected to a straight line at the top surface of the wing at  $y/s = 0.7$ . The lower surface of the wing is a straight line. The body-width-to-wingspan ratio is kept at  $\gamma = 0.7$ , as in previous cases. The  $y$  intersect of the upper surface of the wing is  $x/s = 0.3$ , and the  $y$  intersect of lower surface of the body is  $x/s = -0.7$ . The straight wingtips are moved downward with an angle of  $\psi = -33.69^\circ$ .

The locations of the stationary symmetric vortex pair and the corresponding eigenvalues for the different  $K$  values are shown in



a) Wing-Body cross section and vortex locations



b) Maximum real part of eigenvalues

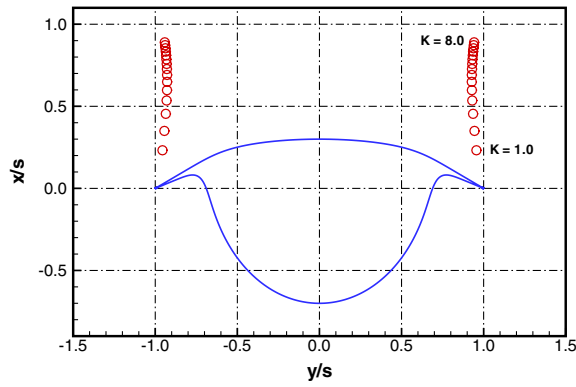
Fig. 8 Straight wing and body combination with the wingtips moved downward.

Figs. 9a and 9b, respectively. The symmetric vortex pair lies almost vertically above the wingtips but not very close to the wingtips, even for small  $K$  values. The maximum eigenvalues are negative for all  $K$  values up to 7.5 and remain very close to zero for  $K > 7.5$ , indicating that the vortices are stable for all angles of attack until  $K$  reaches 7.5 and remain almost neutrally stable, even beyond  $K = 7.5$ . The cobra-like configuration yields the largest range of stable  $K$  among all configuration types studied in this paper. As an example, a cobra-like wing-body combination with a wing with an  $82^\circ$  sweep angle can hold the vortex symmetry until the angle of attack is as high as  $47^\circ$  (assuming no vortex breakdown occurs).

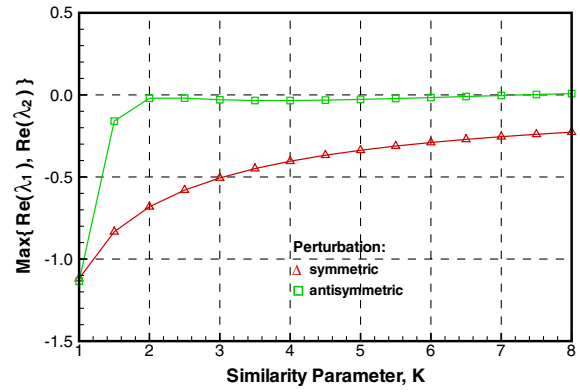
**E. Numerical Verification**

To verify the previous analytical result, a three-dimensional time-accurate Euler solver is used to compute the separation vortex flows and track the motion of the vortices under imposed disturbances. Euler equations are used, since the present study is based on an inviscid model of the vortices, and there is no ambiguity in the location of flow separation because of the sharp leading edges of the wing. Viscous effects can be neglected as a first approximation in the present study. It must be pointed out, however, that viscous effects may generate secondary separation vortices, which can have an influence on the solution and on the stability of the vortices for certain configurations. The flow solver and the computational approach to test the vortex stability have been presented in detail in [14] along with validations and various practical examples. The numerical approach is summarized next and then applied to study the cobra-like configuration.

The flow solver is based on a multiblock, multigrid, second-order finite volume method and parallel code for the steady and unsteady Euler equations. Very stringent convergence criterion is enforced in the computations, and the code strictly preserves symmetry. Given



a) Wing-Body cross section and vortex locations



b) Maximum real part of eigenvalues

Fig. 9 Cobralike wing-body combination.

symmetric initial and boundary conditions, the computations using the steady-flow mode of the solver yield a stationary symmetric vortex-flow solution. The steady-state solutions are used as the initial condition, and the time-accurate Euler solver is used to simulate the flow evolution under a small temporal asymmetric perturbations.

The analysis in the proceeding subsection predicts that the stationary symmetric vortex pair is stable for  $K < 7.5$ . To verify the theoretical prediction, a typical case is chosen:  $\epsilon = 8$  and  $\alpha = 40^\circ$ , corresponding to  $K = 5.971$ .

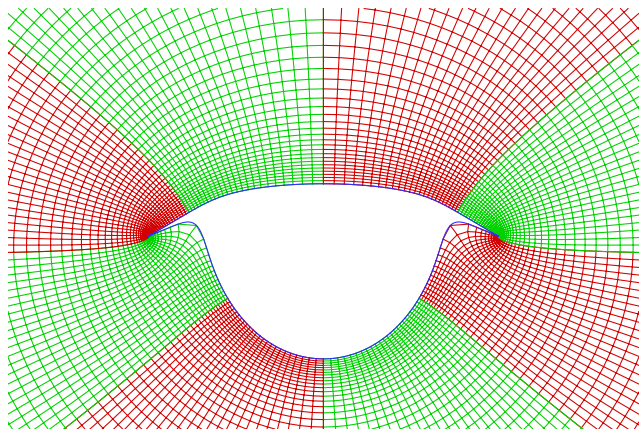
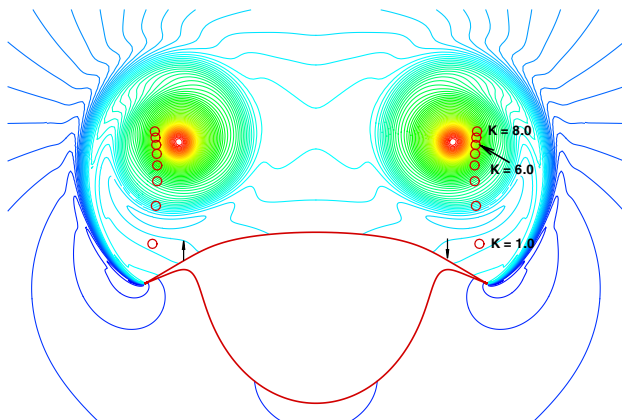


Fig. 10 Computational grid for the cobralike forebody in the exit plane.

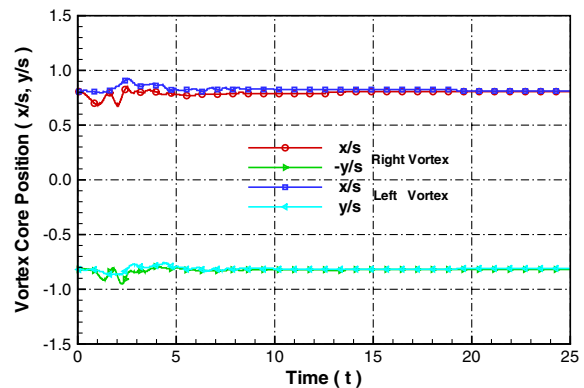
A conical grid consisting of  $5 \times 256 \times 979$  grid points along the longitudinal, radial, and circumferential directions is used. An extraordinarily fine grid in the crossflow plane is needed to resolve the high vorticity regions and simulate the vortex interactions and flow instability. The changes along the body axis are relatively small; therefore, fewer grid points in that direction may be used. Figure 10 shows the grid on the exit plane,  $z = 7.11s$ . The grid is bounded by a circle of radius  $40s$ , where  $s$  is the local semispan. Only every fourth line is shown in the radial and circumferential directions for clarity.

Figure 11a reproduces, from Fig. 9, the body cross-sectional shape and the theoretically predicted locations of the vortices for the various  $K$  values. The numerically computed contours of the longitudinal velocity component are overlaid in the same figure. These contours clearly depict the locations of the vortex centers and the roll up of the separation vortex sheets from the sharp leading edges of the wing. At the vortex core, the longitudinal velocity component reaches its maximum value at about four times that of the freestream velocity ( $u/U_\infty = 4.0926$ ). The pressure coefficient there reaches  $-19.95$ . The computed vortex center at  $K = 5.971$  appears to be slightly inboard compared with the theoretically predicted location at  $K = 6.0$  (pointed at by the long arrow on the right). The difference is attributed to the neglect of the vortex sheets in the theory.

To investigate the stability of the stationary symmetric vortex pair, the converged symmetric solution is then used as the initial condition, and the flow solver is run in time-accurate mode to simulate the evolution of the original symmetric flow subject to a small asymmetric perturbation of a short duration. Asymmetric perturbations are applied because they are found to be the most unstable mode. The small asymmetric perturbations are temporal



a) Contour of Longitudinal Velocity Component and Location of Vortices



b) Time history of vortex center location

Fig. 11 Numerical computations of the cobralike forebody.

suction and blowing on the right and left sides of the wing upper surface, respectively. The suction and blowing locations are shown by the arrows on the top surface of the body in Fig. 11a. The perturbations are activated in the time period  $0 < t < 1$  of the time-accurate computation, where  $t$  is a nondimensional time. The evolution of the coordinates of the computed vortex cores ( $x/s$  and  $y/s$ ) against the nondimensional time  $t$  are recorded and plotted in Fig. 11b. The initially disturbed vortex pair returns to its original symmetric positions after the nondimensional time  $t$  reaches 20. The computational result confirms the previous analytic prediction that the vortices are stable.

#### IV. Conclusions

The stability theory of [11–15] is further developed with the help of a numerical conformal mapping technique to study the stability of the stationary symmetric vortex pair over slender conical bodies of almost arbitrary cross sections at high angles of attack and low speeds. A number of typical cross-sectional configurations of slender conical wing, body, and wing–body combinations have been investigated systematically by the theory. A numerical computational approach using a three-dimensional time-accurate Euler code is used to confirm the analytic findings. The following conclusions are drawn:

1) Downward movement of the wingtips can keep the symmetric vortex pair stable up to a higher angle of attack than upward movement. However, the tip portion of the wing has to be straight in order to avoid a possible occurrence of instability at low angles of attack.

2) Making the upper volume smaller for a body or wing–body combination can keep the symmetric vortex pair stable up to a higher angle of attack.

3) A forebody shape resembling that of a disturbed cobra appears to be an optimal topology to keep the symmetric vortex pair stable in a large range of the Sychev similarity parameter.

#### Acknowledgment

The first author received support for this work by the National Natural Science Foundation of China (grant 10972183).

#### References

- [1] Allen, H. J., and Perkins, E. W., "A Study of the Effects of Viscosity on the Flow over Slender Inclined Bodies of Revolution," NACA TR 1048, 1951.
- [2] Hunt, B. L., "Asymmetric Vortex Forces and Wakes on Slender Bodies," AIAA Paper 1982-1336, Aug. 1982.
- [3] Ericsson, L., and Reding, J., "Asymmetric Flow Separation and Vortex Shedding on Bodies of Revolution," *Tactical Missile Aerodynamics: General Topics*, edited by M. Hemsh, Vol. 141, Progress in Astronautics and Aeronautics, AIAA, Washington, D. C., 1992, pp. 391–452.
- [4] Champigny, P., "Side Forces at High Angles of Attack: Why, When, How?," *La Recherche Aeronautique : Bulletin Bimestriel de l'Office National D'etudes et de Recherches Aeronautiques*, No. 4, 1994, pp. 269–282.
- [5] Malcolm, G., "Forebody Vortex Control," *Progress in Aerospace Sciences*, Vol. 28, No. 3, 1991, pp. 171–234. doi:10.1016/0376-0421(91)90005-0
- [6] Malcolm, G., "Forebody Vortex Control: A Progress Review," AIAA Paper 1993-3540, Aug. 1993.
- [7] Williams, D., "A Review of Forebody Vortex Control Scenarios," AIAA Paper 1997-1967, June 1997.
- [8] Liu, F., Luo, S., Gao, C., Meng, X., Wang, J., and Zhao, Z., "Flow Control over a Conical Forebody Using Duty-Cycled Plasma Actuators," *AIAA Journal*, Vol. 46, No. 11, Nov. 2008, pp. 2969–2973. doi:10.2514/1.39435
- [9] Coe, P., Chambers, J., and Letko, W., "Asymmetric Lateral-Directional Characteristics of Pointed Bodies of Revolution at High Angle Of Attack," NASA TN D-7095, Nov. 1972.
- [10] Siciari, M. J., "Asymmetric Separated Flows at Supersonic Speeds," AIAA Paper 1990-0595, Jan. 1990.
- [11] Cai, J., Liu, F., and Luo, S., "Stability of Symmetric Vortices in Two-Dimensions and over Three-Dimensional Slender Conical Bodies," *Journal of Fluid Mechanics*, Vol. 480, No. 4, April 2003, pp. 65–94. doi:10.1017/S0022112002003567
- [12] Cai, J., Luo, S., and Liu, F., "Stability of Symmetric and Asymmetric Vortex Pairs over Slender Conical Wings and Bodies," *Physics of Fluids*, Vol. 16, No. 2, Feb. 2004, pp. 424–432. doi:10.1063/1.1637601
- [13] Cai, J., Luo, S., and Liu, F., "Stability of Symmetric and Asymmetric Vortices over Slender Conical Wing–Body Combinations," *AIAA Journal*, Vol. 44, No. 7, July 2006, pp. 1601–1608. doi:10.2514/1.19677
- [14] Cai, J., Tsai, H., Luo, S., and Liu, F., "Stability of Vortex Pairs over Slender Conical Bodies: Analysis and Numerical Computation," *AIAA Journal*, Vol. 46, No. 3, March 2008, pp. 712–722. doi:10.2514/1.33498
- [15] Cai, J., Tsai, H.-M., Luo, S., and Liu, F., "Vortex Core and its Effects on the Stability of Vortex Flow over Slender Conical Bodies," AIAA Paper 2005-0062, Jan. 2005.
- [16] Legendre, R., "Écoulement au Voisinage de la Pointe Avant D'une Aile a Forte Flèche aux Incidences Moyennes," *Recherche Aeronautique, Bulletin Bimestriel*, Vol. 30, 1952, pp. 3–8.
- [17] Sychev, V., "Three-Dimensional Hypersonic Gas Flow past Slender Bodies at High Angle Of Attack," *Journal of Mathematics and Mechanics*, Vol. 24, No. 2, Feb. 1960, pp. 296–306. doi:10.1016/0021-8928(60)90033-2
- [18] Hemsch, M. J., "Engineering Analysis of Slender-Body Aerodynamics Using Sychev Similarity Parameters," *Journal of Aircraft*, Vol. 25, No. 7, July 1988, pp. 625–631. doi:10.2514/3.45633
- [19] Hemsch, M. J., "Similarity of High-Angle-of-Attack Subsonic/Transonic Slender-Body Aerodynamics," *Journal of Aircraft*, Vol. 26, No. 1, Jan. 1989, pp. 56–66. doi:10.2514/3.45723
- [20] Barnwell, R. W., "Extension of Hypersonic, High-Incidence, Slender-Body Similarity," *AIAA Journal*, Vol. 25, No. 11, Nov. 1987, pp. 1519–1522. doi:10.2514/3.9816
- [21] Hemsch, M. J., and Luckring, J. M., "Connection Between Leading-Edge Sweep, Vortex Lift, and Vortex Strength for Delta Wings," *Journal of Aircraft*, Vol. 27, No. 5, May 1990, pp. 473–475. doi:10.2514/3.25305
- [22] Traub, L. W., "Simple Prediction Method for Location of Vortex Breakdown on Delta Wings," *Journal of Aircraft*, Vol. 33, No. 2, Feb. 1996, pp. 452–454. doi:10.2514/3.46963
- [23] James, R. M., "A New Look at Two-Dimensional Incompressible Airfoil Theory," Douglas Aircraft Co. Rept. MDC J0918/01, 1971.
- [24] Halsey, N. D., "Potential Flow Analysis of Multielement Airfoils Using Conformal Mapping," *AIAA Journal*, Vol. 17, No. 12, Dec. 1979, pp. 1281–1288. doi:10.2514/3.61308
- [25] Stahl, W., Mahmood, M., and Asghar, A., "Experimental Investigations of the Vortex Flow on Delta Wings at High Incidence," *AIAA Journal*, Vol. 30, No. 4, 1992, pp. 1027–1032. doi:10.2514/3.11023
- [26] Huang, M. K., and Chow, C. Y., "Stability of Leading-Edge Vortex Pair on a Slender Delta Wing," *AIAA Journal*, Vol. 34, No. 6, June 1996, pp. 1182–1187. doi:10.2514/3.13210
- [27] Cai, J., Tsai, H.-M., Luo, S., and Liu, F., "Design Of Wing–Body Configurations to Delay the Onset of Vortex Asymmetry," AIAA Paper 2006-3319, June 2006.

A. Tumin  
Associate Editor